

LATERALLY PROPAGATING DETONATIONS IN THIN HELIUM LAYERS ON ACCRETING WHITE DWARFS

DEAN M. TOWNSLEY¹, KEVIN MOORE², AND LARS BILDSTEN^{2,3},

Draft version October 30, 2018

ABSTRACT

Theoretical work has shown that intermediate mass ($0.01M_{\odot} < M_{\text{He}} < 0.1M_{\odot}$) Helium shells will unstably ignite on the accreting white dwarf (WD) in an AM CVn binary. For more massive ($M > 0.8M_{\odot}$) WDs, these helium shells can be dense enough ($> 5 \times 10^5 \text{ g cm}^{-3}$) that the convectively burning region runs away on a timescale comparable to the sound travel time across the shell; raising the possibility for an explosive outcome rather than an Eddington limited helium novae. The nature of the explosion (i.e. deflagration or detonation) remains ambiguous, is certainly density dependent, and likely breaks spherical symmetry. In the case of detonation, this causes a laterally propagating front whose properties in these geometrically thin and low density shells we begin to study here. Our calculations show that the radial expansion time of $< 0.1 \text{ s}$ leads to incomplete helium burning, in agreement with recent work by Sim and collaborators, but that the nuclear energy released is still adequate to realize a self-sustaining laterally propagating detonation. These detonations are slower than the Chapman-Jouguet speed of $1.5 \times 10^9 \text{ cm s}^{-1}$, but still fast enough at $0.9 \times 10^9 \text{ cm s}^{-1}$ to go around the star prior to the transit through the star of the inwardly propagating weak shock. Our simulations resolve the subsonic region behind the reaction front in the detonation wave. The 2D nucleosynthesis is shown to be consistent with a truncated 1D Zeldovich-von Neumann-Döring (ZND) calculation at the slower detonation speed. The ashes from the lateral detonation are typically He rich, and consist of predominantly ^{44}Ti , ^{48}Cr , along with a small amount of ^{52}Fe , with very little ^{56}Ni and with significant ^{40}Ca in carbon-enriched layers. If this helium detonation results in a Type Ia Supernova, its spectral signatures would appear for the first few days after explosion.

Subject headings: hydrodynamics — nuclear reactions, nucleosynthesis, abundances — white dwarfs

1. INTRODUCTION

Recent theoretical insights (Bildsten et al. 2007; Shen et al. 2010; Waldman et al. 2010; Woosley & Kasen 2011) and observations of very rapidly evolving thermonuclear supernovae such as 2002bj (Poznanski et al. 2010), SN2010X (Kasliwal et al. 2010), SN 1939B, and SN 1885A (Perets et al. 2011) motivate an investigation of the outcome of unstable burning of intermediate mass ($0.01M_{\odot} < M_{\text{He}} < 0.2M_{\odot}$) Helium shells on accreting white dwarfs (WDs). Shen & Bildsten (2009) showed that the burning initially proceeds as a spherically symmetric slowly evolving (minutes to hours) convective layer [see also Woosley & Kasen (2011)]. For even lower shell masses (such as occur in stars on the Asymptotic Giant Branch), the convective burning causes radial expansion adequate to increase the evolutionary timescales to times long enough for confidence in a one-dimensional hydrostatic calculation. However, there is a critical helium shell mass ($M_{\text{He}} > 0.1(0.01)M_{\odot}$ for a WD mass of $M = 0.6(1.1)M_{\odot}$) above which the convective burning timescales become so short that a dynamical mode of burning will occur (Shen & Bildsten 2009).

As highlighted by many (Bildsten et al. 2007; Shen et al. 2010; Woosley & Kasen 2011), the dynamically burning He shell differs from the well studied case of dynamic carbon burning in WD cores during Type Ia SNe, as the finite gravitational acceleration, g , in the He shell rapidly forces mixing of any unstable density gradients from a radially propagat-

ing deflagration (Timmes & Niemeyer 2000). This prohibits the localization of a well defined and propagating deflagration front. If detonation is the result, we expect that a lack of synchronicity across the star will lead to laterally propagating detonation wave(s) from the ignition site(s). Fink et al. (2007, 2010); Sim et al. (2012) revived the exciting possibility (Livne & Glasner 1991; Woosley & Weaver 1994; Livne & Arnett 1995) that the weak shock that penetrates the underlying WD from a laterally propagating He detonation will strengthen enough (even for a $M_{\text{He}} = 0.01M_{\odot}$ shell) at the off-center focus point to trigger a C/O detonation in the WD. They have argued that nearly all He detonations will lead to a complete explosion of sub-Chandrasekhar C/O mass WDs. This motivated theoretical modeling of such explosive events (Sim et al. 2010; Kromer et al. 2010; Waldman et al. 2010; Woosley & Kasen 2011; Sim et al. 2012) finding similarities to the width-luminosity relation of Type Ia SNe and potentially offering new insights on unusual events [e.g. SN 2005E (Perets et al. 2010), PTF09dav (Sullivan et al. 2011), and others (Kasliwal et al. 2011)]

Though uncertainties remain (Shen et al. 2010; Woosley & Kasen 2011) as to the exact criteria that must be met to initiate a detonation in these lower density ($\rho < 10^6 \text{ g cm}^{-3}$) He shells, we work here to resolve how the lateral propagation will be impacted by the radial expansion that occurs during the burning. The radial blow-out timescale is $H/c_s \sim 0.01 \text{ s}$ for a shell of thickness $H \approx 10^7 \text{ cm}$, where the sound speed, $c_s \approx 10^9 \text{ cm s}^{-1}$, is set by the post-shock temperature of the detonation front. This timescale decreases for thinner layers, whereas the nuclear burning timescale in the detonation reaction zone increases. If a propagating detonation wave remains stable under incomplete burning, it would reduce the propagation speed to values lower than the Chapman-Jouguet (CJ)

¹ Department of Physics and Astronomy, University of Alabama, Tuscaloosa, AL; Dean.M.Townsley@ua.edu

² Department of Physics, University of California, Santa Barbara, CA

³ Kavli Institute for Theoretical Physics, University of California, Santa Barbara, CA

speed of 1.5×10^9 cm s⁻¹ calculated for a complete burn of He to ⁵⁶Ni (Sim et al. 2012). At even lower densities (or shell thicknesses), the blow-out occurs so rapidly that the propagation could be quenched.

We begin in §2 by showing a 2D simulation of a steadily propagating detonation in a thin helium layer for an example case motivated by the AM CVn accretion scenario. In order to investigate the robustness of our numerical techniques and better understand the incomplete burning that occurs, we undertake two sets of comparisons. In §3, we perform 1D and 2D simulations, with enough resolution to resolve all the burning scales, investigating transient strengthening detonations in uniform pure He. We find that the incompletely burned strengthening detonation provides a useful comparison to the blowout case. In §4, we compare our simulations to integrations that give the structure of 1D steady-state detonations (ZND⁴) performed with a large (200-nuclide) reaction network and find qualitative agreement. Finally, in §5, we discuss astrophysical implications and future work.

2. SURFACE BLOWOUT INDUCES FREEZE-OUT OF INTERMEDIATE PRODUCTS

Our fiducial model for the multidimensional runs was motivated by a time dependent \dot{M} calculation with MESA⁵ (Paxton et al. 2011) that had a declining \dot{M} as expected from a degenerate He donor in an AM CVn binary (Bildsten et al. 2006, 2007). This exploratory calculation had 10 He flashes at very high accretion rates on the $M = 1.0M_{\odot}$ WD, with about two-thirds of the accreted material leaving during the He novae. The remaining carbon-oxygen ashes from the He burning creates a hot ($T \approx 8 \times 10^7$ K) layer of $\approx 0.015M_{\odot}$. The final flash occurred when $\dot{M} \approx 6 \times 10^{-8}M_{\odot} \text{ yr}^{-1}$, with a freshly accumulated helium layer mass of $0.028M_{\odot}$. At this \dot{M} , the temperature maximum occurs above the base of the He shell, placing the base of the convective zone at a mass coordinate inward from the surface of $0.014M_{\odot}$. Our fiducial model is comparable to two $M = 1.0M_{\odot}$ WD models of Woosley & Kasen (2011). The first (10AA) had a cold C/O core ($T < 3 \times 10^7$ K) and $\dot{M} = 7 \times 10^{-8}M_{\odot} \text{ yr}^{-1}$, giving an accumulated mass of $M_a = 0.052M_{\odot}$ and a convective layer of $0.0262M_{\odot}$, thicker than our He layer due to the colder core. The second (10HB) had a hot C/O core ($T \approx (7-8) \times 10^7$ K) and $\dot{M} = 5 \times 10^{-8}M_{\odot} \text{ yr}^{-1}$, giving an accumulated mass of $M_a = 0.022M_{\odot}$ and a convective layer of $0.022M_{\odot}$, much closer to our fiducial. Compared to the models shown in their Figure 2, our model has a peak luminosity of $10^{46.6}$ erg s⁻¹ when the conditions at the base of the convection zone are $\rho_6 = 0.14$ and $T_8 = 5.0$. This places our model above their threshold for shell detonations.

For our simulation, we used the temperature and density structure when the timescale for temperature change in the convective burning layer was at its minimum, about 5 seconds. This calculation is intended to demonstrate one case in which the burning scales are long enough for blowout to truncate the reactions. This radial (vertical) structure is shown in Figure 1. The initial helium layer is in hydrostatic balance, with the hot ($T_9 = 0.52$), carbon-enriched ($X_{12} = 0.1$ due to He burning) convection zone above the colder ($T_9 = 0.08$) pure

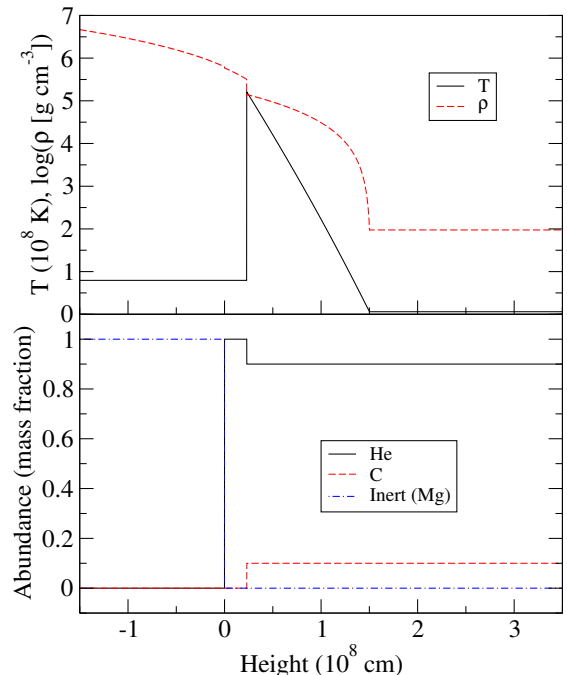


FIG. 1.— Initial vertical profile on the domain of temperature, density and abundances.

He layer. The base of the cold He layer defines the zero of the vertical coordinate, and has a density of $\rho_5 = 5.89$. The cold layer extends up to $\approx 0.25 \times 10^8$ cm, and has a column depth of 10^{13} g cm⁻² or $\approx 0.01M_{\odot}$, while the convective layer extends to $\approx 1.4 \times 10^8$ cm and has a similar mass. Above this is a low-density "fluff" layer outside the star extending to the edge of the grid. We work in plane parallel, with $g = 7.32 \times 10^8$ cm s⁻², appropriate to the $1M_{\odot}$ WD of radius $R = 4.3 \times 10^8$ cm. The helium is sitting on a presumed (for this simulation) inert core.

Reactive hydrodynamics simulations were performed using FLASH⁶ (Fryxell et al. 2000) and utilized the "approx13" nuclear reaction network (Timmes et al. 2000a) that accounts for the fast $(\alpha, p)(p, \gamma)$ side channels relevant to alpha burning (Timmes et al. 2000b). We used the piecewise parabolic method (PPM; Colella & Woodward 1984) for compressible hydrodynamics. Reactions were disabled in regions of the grid within a detected shock (Fryxell et al. 1989). The hydrodynamic and reaction evolution are operator split and the temperature is held fixed during the reactions. A hydrostatic lower boundary condition is used (Zingale et al. 2002), implemented by Townsley and included in FLASH 3.3. The plane-parallel calculation is performed with a uniform 1.22×10^5 cm grid of cells with large lateral width of 5×10^8 cm. We do not initialize any convective motion, rather we just use the thermal profile implied by a constant entropy and abundance convective zone.

We numerically initiate the detonation by raising the temperature in the convective zone to $T_9 = 3$ in a circular region of radius 10^7 cm, centered 1.2×10^7 cm above the base of the convective layer. This does not directly ignite a detonation, but rather creates a shock wave that traverses the cold layer; reflects from the inert core, and emerges out as a detonation wave.⁷ The resulting detonation front is shown in Figure 2,

⁴ Throughout we use Zeldovich-von Neumann-Döring (ZND) to refer to the eigenvalue method for computing the spatial structure of steady state detonations. See, e.g., Khokhlov (1989) for a convenient form of the equations integrated and Fickett & Davis (1979) for a broader discussion.

⁵ <http://mesa.sourceforge.net>

⁶ <http://flash.uchicago.edu>

⁷ This brings up a shortcoming of this calculation, which is that this inter-

which shows a snapshot of the detonation propagation 0.5 seconds after the detonation was ignited at $x = 4.5 \times 10^8$ cm. The large lateral width of our simulation allows for the detonation wave to propagate far from the initiation site, demonstrating a steady-state form of much smaller spatial dimensions ($\lesssim 10^7$ cm). The resulting speed of the detonation front is shown in Figure 3 by the points labelled “Blowout” and reaches 8.7×10^8 cm s⁻¹ for several tenths of a second as it crosses our large domain.

The resulting composition profiles are shown in Figure 2. The burning is far from complete, with the ⁴He abundance far behind the detonation front only falling to ≈ 0.5 . Scarcely any ⁵⁶Ni is produced, while more significant amounts of slightly lower *Z* elements are made, including ⁴⁸Cr (bottom middle panel) and ⁴⁴Ti, but relatively little ⁵²Fe (not shown). The nucleosynthesis in the hot, carbon-enriched layer gives a similar amount of unburned helium, producing generally lower *Z* products such as ⁴⁰Ca (lower left panel), and appears to be a detonation wave partially supported by the overpressure from the underlying detonation. We performed a similar calculation in which the overlying layer had no carbon, and the detonation speed was slightly lower, 8.5×10^8 cm s⁻¹, but all other features were qualitatively similar. The detonation front (vertically extending to 0.5×10^8 cm) is cellular, with the strongest shock-fronts propagating at an angle with respect to the overall leftward velocity. These cross-propagating shocks traverse both the cold pure helium and the carbon enriched layer above.

We hypothesize that the surface blowout has induced a eigenvalue-type (sometimes called “pathological”) detonation solution (Fickett & Davis 1979) in which the sonic point, where the flow becomes supersonic with respect to the shock front, is inside the reaction zone. This truncates the burning while still preserving a self-propagating detonation structure between the shock front and the sonic point (actually sonic locus in multiple dimensions). This is surprising, as discussed below in Section 3, a detonation in uniform pure helium at the density at the base of the helium layer has a ZND length (to reach pure ⁵⁶Ni) much longer than our grid.

3. LARGE AND TRANSIENT DETONATION STRUCTURES

As we have shown (see also Sim et al. 2012), the low helium densities near the WD surface allow matter to blowout on a timescale comparable to the burning time. This is in contrast with earlier work done on Helium detonations in denser environments. For example, Khokhlov (1989) performed ZND calculations for pure helium at $\rho_5 = 50$, finding complete burning by the time (and distance, 10^8 cm) the flow behind the detonation front reaches the sonic point and a speed, 1.5×10^9 cm s⁻¹, consistent with the Chapman-Jouget (CJ) value for complete burning. However, at lower densities, the detonation structures become much larger than the vertical (and even horizontal) scale of the outer layers of a WD (Timmes & Niemeyer 2000), requiring a new approach. It also raises the possibility that a propagating detonation is not even possible in these thin helium layers, a quenching outcome well known in chemical detonations.

We begin by investigating how marginally ignited detonations strengthen towards the steady-state CJ solution and how

this depends on composition. At low densities, these solutions will extend to physical dimensions much larger than can be accommodated on a WD, but will enable comparisons to ZND calculations that help us understand the likely effects of a finite geometry. In order to facilitate direct comparison with ZND calculations, we work in a 1-dimensional plane parallel geometry in a medium of uniform density, temperature (typically at $T_9 = 0.1$) and composition, sometimes including a small carbon fraction. The detonation is ignited by setting the temperature close to the boundary at $T_9 = 3$ with a discontinuous fall to the ambient temperature. We usually use the smallest hot region that leads to a propagating detonation, decrementing a factor of 10 at a time. We perform these simulations at two different resolutions, a coarse resolution to allow the detonation to reach steady state, and a fine resolution which resolves all the burning stages. Adaptive mesh refinement is used in all cases, so that the resolution is actually the minimum cell size.

We start by comparing to Khokhlov (1988, 1989)’s calculations at $\rho_5 = 50$ and $T_9 = 0.2$ for the initial state. The speed at which the shock front propagates as the 10^5 cm resolution simulation progresses is shown by the black curve in Figure 3. This detonation is of the CJ-type and the CJ speed (as determined by a calculation containing only the 13 α -chain elements) is shown by the horizontal dashed line at a speed of 1.54×10^9 cm s⁻¹. This is also the speed obtained by interpolating in Table IV in Khokhlov (1988), and we confirm his spatial profiles. Though it only takes 0.01s to reach 80% of the CJ speed, the full speed is not attained for about one second.

We now consider a case with $\rho_5 = 5$, similar to the surface detonation calculation presented above. The evolution of the shock velocity (solid red) is shown in Figure 3, and is qualitatively similar to the higher density result. Note that there are two red curves, one at a coarse (4.8×10^6 cm) resolution and one much finer resolution (1000 cm). We performed the fine resolution simulations at a variety of ignition sizes, finding that ignition sizes of 10^5 cm and below fail to produce a propagating detonation. We therefore use an ignition size of 10^6 cm for all the fine simulations shown here. Similar to the higher density result, this calculation asymptotes to the CJ speed, but only after 1000 seconds and a propagation length $\approx 10^{12}$ cm, larger than the whole WD.

We also explored the effects of a modest fraction of ¹²C in the fuel, which Shen & Bildsten (2009) suggested may provide a faster reaction channel via ¹²C(α, γ)¹⁶O. We performed simulations with $X_{12} = 0.05$ and 0.1, shown by the blue and magenta curves in Figure 3. Before about 10^{-3} s, the shock velocity is that of the leading shock from our ignition, not yet a detonation. The region between the contact discontinuity at the edge of our ignition region and this leading initiation shock is effectively preconditioned by the shock propagation, and runs away to ignite the detonation. The spike in propagation speed at a few $\times 10^{-3}$ s is when this newly-formed detonation first passes the leading shock. It leaves this pre-heated region with an enhanced speed due to the preheating, falling quickly as the detonation propagates into now unheated fuel. Due to the presence of carbon, there is a continued enhancement of the propagation speed up to about 0.1 s, potentially relevant if carbon is present in the accumulated cold He layer. As the detonation continues to strengthen, the speed becomes dominated by the consumption of ⁴He, and asymptotes toward

action led to immediate ignition of C/O when we allowed for carbon fusion. This is an artifact of our initiation scheme, and led us to use ²⁴Mg for the underlying layer in this initial study.

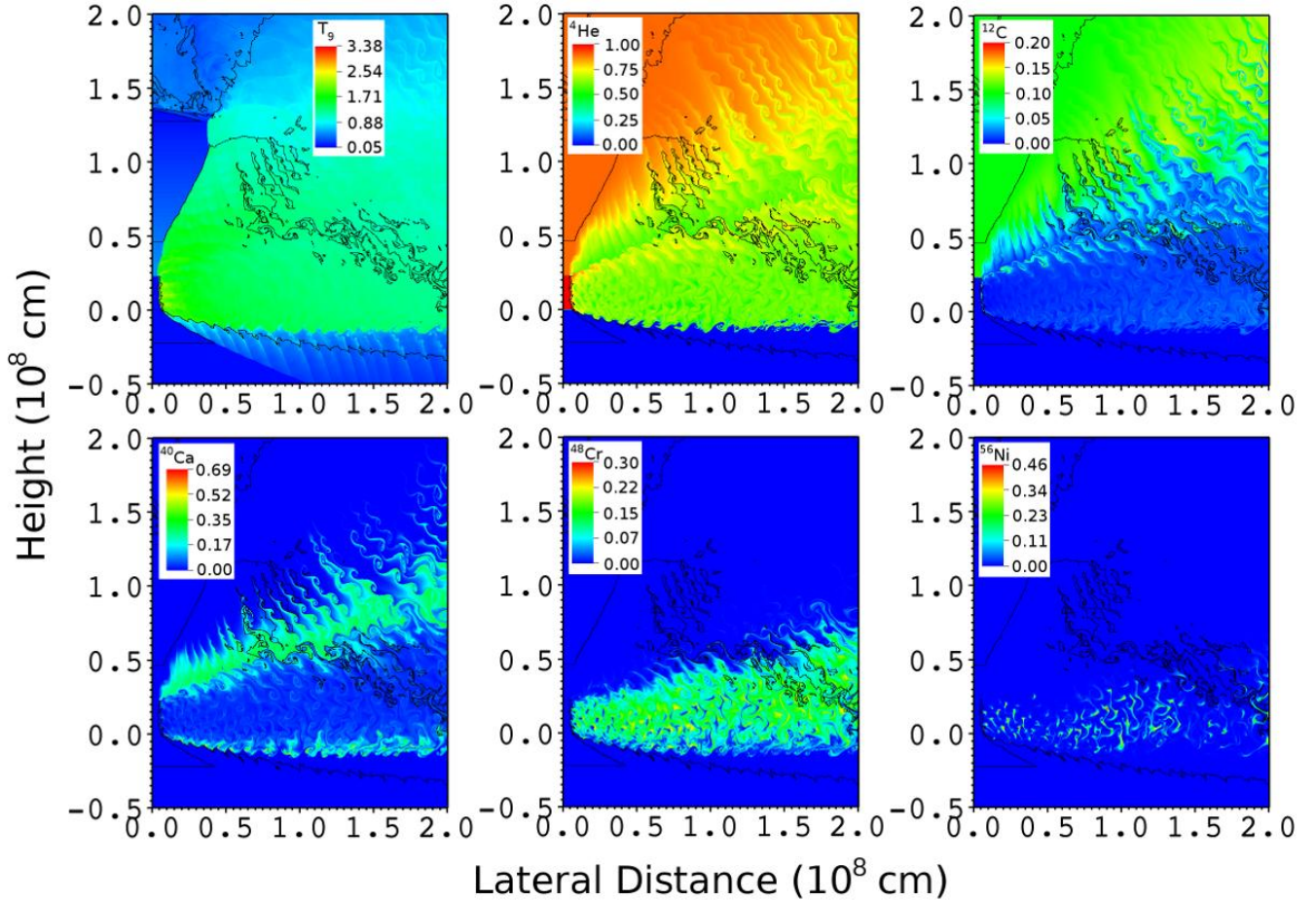


FIG. 2.— Steady-state temperature and abundance (in mass fractions) structure of a surface detonation propagating from right to left in the accreted helium layer of a WD. Prior to ignition, a hot, actively burning convection zone (0.25-1.4 on the vertical (radial) axis) enriched in ^{12}C ashes sits above a cold helium layer (0.0-0.25) atop an inert core. Density contours are shown at 10^3 , 10^4 , 10^5 and 10^6 g cm^{-3} . This snapshot is from 0.5 s after the detonation was ignited at $x = 4.5 \times 10^8$ cm. Only a portion of the computational domain near the detonation front is shown.

the CJ solution.

To investigate the cellular structure of these detonation fronts, we also performed a 2-dimensional calculation. The configuration was plane-parallel in a uniform medium, but now with random 1% density perturbations near the ignition front to seed the cellular instability. The domain width transverse to the detonation front was 10^7 cm with periodic boundary conditions, adequate to accommodate several detonation cell widths, though the cell width appeared to grow with time as the detonation strengthened. The resolution for the 2-d simulation was about 5000 cm, enough to marginally resolve the fastest stage, helium capture on produced carbon. Even so, the evolution of the detonation speed (green curve in Figure 3) agrees quite well with the 1-d simulations, giving us confidence that our 1-d simulations are robust enough to compare to the inherently multi-dimensional blowout case.

This 2-dimensional uniform density simulation also allows us to study resolution effects in a more controlled context. By comparing a calculation at 7.8×10^4 cm resolution to the one at 5000 cm, it appears that size of the cellular structure is influenced by resolution, with larger distance between cross-propagating shock fronts at coarser resolutions. However this does not have a significant impact on the resolved nucleosynthetic structures such as for the higher- Z elements (i.e. Ca, Ti, Cr, Fe and Ni).

We find that weakly ignited (initially underdriven) detona-

tions in helium strengthen toward the steady-state solution over time, but if the overall detonation structure – that is the thermodynamic and compositional profiles in space – is large, it will take a significant run of space for the detonation to take on this steady state structure. The incomplete burning structure created by the blowout near the WD surface is similar to the early phases of these strengthening detonations, providing a valuable comparison.

4. VERIFICATION BETWEEN ZND CALCULATIONS AND FLASH SIMULATIONS

We have established that the helium detonation blowout at low densities reduces the available burning time, inhibiting the complete burning of helium and highlighting the importance of accurately calculating the production of intermediate mass products. We begin by exploring how the details of the reaction network and calculation method impact the nucleosynthesis. So as to save computational time, the FLASH calculation uses the “approx13” (Timmes et al. 2000a) reaction network, a simplified 13 nuclide network with steady-state approximations of heavier p -rich nuclei along $(\alpha, p)(p, \gamma)$ channels and their inverses. We check whether this approximation leads to any substantial nucleosynthetic differences by comparing to 1D ZND calculations performed with a 200 nuclide nuclear network.

In a standard ZND computation, the eigenvalue detonation

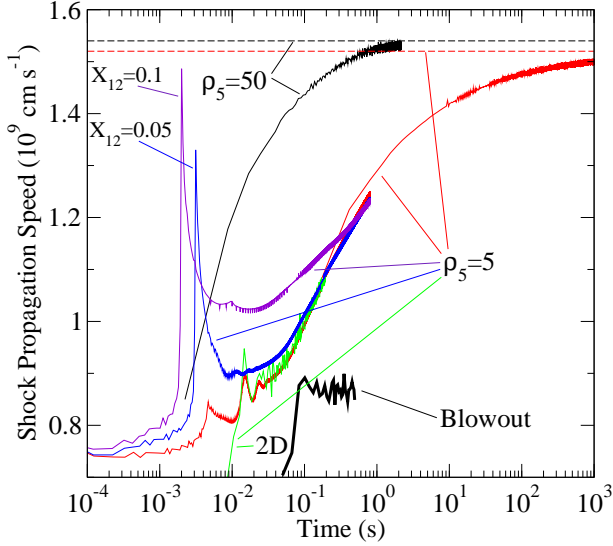


FIG. 3.— Detonation shock velocity as a function of time for detonations in helium. Two densities for uniform fuel are shown, $5 \times 10^6 \text{ g cm}^{-3}$ (solid black) and $5 \times 10^5 \text{ g cm}^{-3}$ (1D: solid red, 2D: green), and dashed lines show the corresponding steady state CJ speeds. The speed for material containing some ^{12}C in fuel, $X_{12} = 0.05$ (blue) and $X_{12} = 0.1$ (purple) is initially higher but asymptotes to similar behavior. The propagation speed of the detonation wave moving through the helium surface layer on a WD (thick black) stabilizes well below the CJ speed.

speed (or, equivalently, shock strength) is obtained when the position in the flow where the heat release function (see e.g. Khokhlov 1989) is zero coincides with the flow velocity being sonic with respect to the shock front. This gives a physically consistent transition from the detonation structure to the following flow beyond the sonic locus. However, we cannot perform a standard ZND computation for anything but the true steady state, which in this case is a far stronger detonation than either the early transient or blowout cases. Instead, we perform the first portion of a ZND integration, starting from the shock, for the known shock strength drawn from simulations and truncate our integration near the sonic point where it would become singular.

The first step is to examine the nucleosynthetic differences between a ZND calculation with approx13 and the 200 nuclide nuclear network at the same conditions ($\rho_5 = 5$ and $T_8 = 1$). We choose to initialize the comparison ZND integrations with the detonation velocity achieved at 0.2 seconds in the high resolution uniform medium 2D FLASH run, $1.09 \times 10^9 \text{ cm s}^{-1}$. This velocity is still lower than the steady-state CJ detonation velocity, therefore the ZND integration will terminate when the downstream velocity in the shock frame is equal to the sound speed, here at a distance of $4 \times 10^6 \text{ cm}$. The resulting nuclide abundance distributions are shown in Figure 4, showing that approx13 provides a suitable reproduction of the results obtained from the 200 nuclide network. ^{44}Ti is overproduced by about a factor of two at intermediate length scales, indicating that this nuclide is likely slightly overpredicted in our yields.

A next check is to verify that the intermediate element production is consistent between the uniform density simulations and the ZND integration, both using the approx13 network. We compare, in Figure 5, the simulation (dotted line for 1D), which captures the beginning phase of the detonation while the shock is still strengthening, to the truncated ZND integration (solid line for ZND). The excellent comparison shows

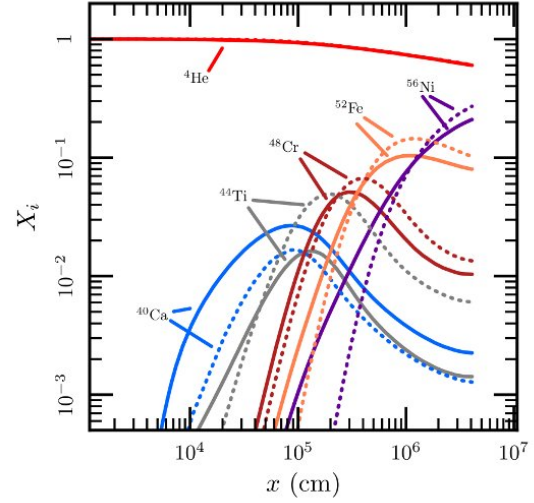


FIG. 4.— Comparison of post-shock nucleosynthesis of detonations in pure He computed in the ZND formalism using two different reaction networks. The dotted lines are calculated using the approx13 reaction network and the solid lines from the 200-isotope network. The detonation velocity was $D = 1.09 \times 10^9 \text{ cm/s}$ for each run and the ambient conditions were $\rho_0 = 5 \times 10^5 \text{ g cm}^{-3}$ and $T_0 = 10^8 \text{ K}$.

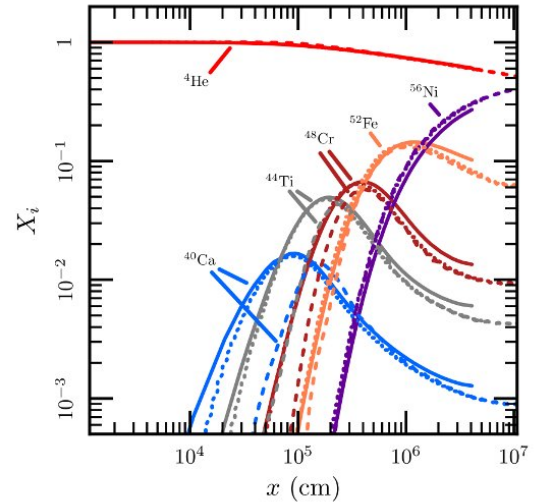


FIG. 5.— Comparison of laterally averaged 2-dimensional (dashed) and 1-dimensional (dotted) FLASH simulations of the He detonation structure after 0.2 s of propagation. Also shown is a ZND calculation (solid), which uses the FLASH detonation speed at 0.2 s, $1.09 \times 10^9 \text{ cm s}^{-1}$. Ambient conditions were $\rho_0 = 5 \times 10^5 \text{ g cm}^{-3}$ and $T_0 = 10^8 \text{ K}$. Both FLASH and ZND are using the approx13 reaction network.

that the truncated ZND is a suitable approach to understanding the strengthening detonations. Additionally, we need to relate the 2D simulations to those in 1D. The laterally averaged 2D results are shown by the dashed line in Figure 5, remarkably similar to the 1D results. Apparently the cellular nature of the 2D detonation did not significantly change the burning length scale from the 1D case.

We have shown consistency in the detonation structure

computed by all of the following: (1) a truncated ZND calculation with a large network, (2) a truncated ZND calculation with the `aprox13` network, (3) 1D hydrodynamic simulations of the transient phase of a strengthening detonation that resolve all relevant reaction length scales, (4) 2D hydrodynamic simulations that nearly resolve all relevant length scales. These consistencies give us confidence in the propagating solution revealed by the blowout simulations, but we have yet to use these truncated ZND calculations to fully diagnose (and maybe predict) the blowout results (both nucleosynthetic yields and speeds).

5. CONCLUSIONS

We have shown that a thin helium layer on the surface of a WD can host a steady-state, laterally propagating detonation at low densities ($< 10^6 \text{ g cm}^{-3}$). Under these conditions, the detonation takes on the character of an eigenvalue-type detonation in which the sonic locus occurs well before complete helium burning is achieved. The stability and compact structure of the resulting detonation is surprising because the size of the reaction zone of a steady-state detonation, which burns to completion, at these densities ($\gg 10^8 \text{ cm}$) is larger than the layer thickness ($\sim 10^7 \text{ cm}$) or even the star itself. Our 2D reactive hydrodynamic simulations resolved the subsonic region behind the shock, exhibited the radial blowout of the hot material, and primarily yielded intermediate mass products (i.e. ^{44}Ti and ^{48}Cr) and relatively little ^{56}Ni . The incomplete burning had a spatial scale much smaller than the vertical thickness of the helium layer, and a detonation speed of $0.9 \times 10^9 \text{ cm s}^{-1}$, lower than the Chapman-Jouget speed of complete burning, $1.5 \times 10^9 \text{ cm s}^{-1}$.

This lower detonation speed reduces the strength of the inwardly moving shock that may ignite a detonation in the carbon-oxygen core and cause a Type Ia SNe (Fink et al. 2007, 2010; Sim et al. 2012). The slower speed moves the convergence point for these weak shocks further towards the surface, potentially making it harder for the carbon to detonate. If a carbon detonation still occurs, the reduction in high-Z elements that we found for the helium layer would allow for colors and spectral features consistent with normal Type Ia SNe over most of their evolution (Kromer et al. 2010; Woosley & Kasen 2011; Sim et al. 2012) for even larger helium layer masses. Modest carbon enrichment in the helium layer was found here to produce significant amounts of ^{40}Ca , which, if the underlying core detonated, would appear in spectra at high velocities with several possible sources of asymmetry, a common feature of SNIa (Kasen et al. 2003; Mazzali et al. 2005; Tanaka et al. 2008; Foley et al. 2012). It is certainly the case that the extremely low-mass helium shell considered here would only effect the earliest time colors (Woosley & Kasen 2011; Piro 2012), highlighting the importance of obtaining early observations of SNe Ia (Nugent et al. 2011; Foley et al. 2012).

If the carbon does not detonate, then the only observable signatures would be from the ejected ashes of the helium detonation (Bildsten et al. 2007; Shen et al. 2010), a “Ia” supernovae. For this $M = M_{\odot}$ WD, the gravitational binding energy of the material at the surface is $3 \times 10^{17} \text{ ergs g}^{-1}$, and rough integrals over the 2D simulation yielded burning products of $X_4 = 0.66$, $X_{12} \approx 0.054$, $X_{40} \approx 0.066$, $X_{44} = 0.079$, $X_{48} \approx 0.053$, $X_{52} = 0.026$, $X_{56} = 0.0067$, and a smattering of other elements. This incomplete burning releases $\approx 4.0 \times 10^{17} \text{ erg g}^{-1}$, so that the ashes are unbound and reach infinity with an average velocity of 4500 km s^{-1} , a rather low velocity compared to normal supernovae. The small ejecta mass ($0.028M_{\odot}$) will lead to a short duration (likely less than 2 days near peak light) and the small amount of long-lived radioactivities imply a low luminosity ($\ll 10^{42} \text{ erg s}^{-1}$). This rather low energy release brings up the interesting possibility that, for thin shells, a detonation might not unbind the surface layers, though the CO interior might still shock-ignite.

There remain several important uncertainties. The greatest is related to the initiation of the detonation in the convective helium burning layer on the WD surface (Shen et al. 2010; Woosley & Kasen 2011). We assumed here that a detonation was ignited and just considered its propagation and stability. We intend to first explore the dependence of the detonation speed on both the He layer thickness and density. Coupled with our truncated ZND calculations (see section 4), we hope that these insights will yield a direct approach to predicting the minimum possible layer that will allow for a propagating detonation. This more complete understanding of the mechanism by which the blowout of the surface layer leads to an eigenvalue-type stable detonation solution should allow for predictions of nucleosynthetic outcomes across a broad range of parameter space without expensive multidimensional simulations.

We thank Ryan Foley for helpful discussions and Bill Paxton for MESA calculations. Some of the software used in this work was in part developed by the DOE-supported ASC/Alliances Center for Astrophysical Thermonuclear Flashes at the University of Chicago. We thank Nathan Hearn for having made his QuickFlash analysis tools publicly available at <http://quickflash.sourceforge.net>. We used Frank Timmes’ nuclear reaction network (<http://cococubed.asu.edu>) for preliminary calculations. Some simulations presented in this work were run on the Ranger supercomputer at the Texas Advanced Computing Center as part of the Extreme Science and Engineering Discovery Environment (XSEDE, formally TeraGrid), which is supported by National Science Foundation grant number OCI-1053575. This research has been supported by the National Science Foundation under grants PHY 11-25915 and AST 11-09174.

REFERENCES

- Bildsten, L., Shen, K. J., Weinberg, N. N., & Nelemans, G. 2007, *ApJ*, 662, L95
 Bildsten, L., Townsley, D. M., Deloye, C. J., & Nelemans, G. 2006, *ApJ*, 640, 466
 Colella, P. & Woodward, P. R. 1984, *Journal of Computational Physics*, 54, 174
 Fickett, W. & Davis, W. C. 1979, *Detonation* (Berkeley: University of California Press)
 Fink, M., Hillebrandt, W., & Röpke, F. K. 2007, *A&A*, 476, 1133
 Fink, M., Röpke, F. K., Hillebrandt, W., Seitenzahl, I. R., Sim, S. A., & Kromer, M. 2010, *A&A*, 514, A53
 Foley, R. J., Challis, P. J., Filippenko, A. V., Ganeshalingam, M., Landsman, W., Li, W., Marion, G. H., Silverman, J. M., Beaton, R. L., Bennert, V. N., Cenko, S. B., Childress, M., Guhathakurta, P., Jiang, L., Kalirai, J. S., Kirshner, R. P., Stockton, A., Tollerud, E. J., Vinkó, J., Wheeler, J. C., & Woo, J.-H. 2012, *ApJ*, 744, 38
 Fryxell, B., Olson, K., Ricker, P., Timmes, F. X., Zingale, M., Lamb, D. Q., MacNeice, P., Rosner, R., Truran, J. W., & Tufo, H. 2000, *ApJS*, 131, 273

- Fryxell, B. A., Müller, E., & Arnett, D. 1989, MPlA Technical Report
- Kasen, D., Nugent, P., Wang, L., Howell, D. A., Wheeler, J. C., Höflich, P., Baade, D., Baron, E., & Hauschildt, P. H. 2003, *ApJ*, 593, 788
- Kasliwal, M. M., Kulkarni, S. R., Gal-Yam, A., Nugent, P. E., Sullivan, M., Bildsten, L., Yaron, O., Perets, H. B., Arcavi, I., Ben-Ami, S., Bhalerao, V. B., Bloom, J. S., Cenko, S. B., Filippenko, A. V., Frail, D. A., Ganeshalingam, M., Horesh, A., Howell, D. A., Law, N. M., Leonard, D. C., Li, W., Ofek, E. O., Polishook, D., Poznanski, D., Quimby, R. M., Silverman, J. M., Sternberg, A., & Xu, D. 2011, *ArXiv e-prints*
- Kasliwal, M. M., Kulkarni, S. R., Gal-Yam, A., Yaron, O., Quimby, R. M., Ofek, E. O., Nugent, P., Poznanski, D., Jacobsen, J., Sternberg, A., Arcavi, I., Howell, D. A., Sullivan, M., Rich, D. J., Burke, P. F., Brimacombe, J., Milisavljevic, D., Fesen, R., Bildsten, L., Shen, K., Cenko, S. B., Bloom, J. S., Hsiao, E., Law, N. M., Gehrels, N., Immler, S., Dekany, R., Rahmer, G., Hale, D., Smith, R., Zolkower, J., Velur, V., Walters, R., Henning, J., Bui, K., & McKenna, D. 2010, *ApJ*, 723, L98
- Khokhlov, A. M. 1988, *Ap&SS*, 149, 91
- . 1989, *MNRAS*, 239, 785
- Kromer, M., Sim, S. A., Fink, M., Röpke, F. K., Seitzzahl, I. R., & Hillebrandt, W. 2010, *ApJ*, 719, 1067
- Livne, E. & Arnett, D. 1995, *ApJ*, 452, 62
- Livne, E. & Glasner, A. S. 1991, *ApJ*, 370, 272
- Mazzali, P. A., Benetti, S., Altavilla, G., Blanc, G., Cappellaro, E., Elias-Rosa, N., Garavini, G., Goobar, A., Harutyunyan, A., Kotak, R., Leibundgut, B., Lundqvist, P., Mattila, S., Mendez, J., Nobili, S., Pain, R., Pastorello, A., Patat, F., Pignata, G., Podsiadlowski, P., Ruiz-Lapuente, P., Salvo, M., Schmidt, B. P., Sollerman, J., Stanishev, V., Stehle, M., Tout, C., Turatto, M., & Hillebrandt, W. 2005, *ApJ*, 623, L37
- Nugent, P. E., Sullivan, M., Cenko, S. B., Thomas, R. C., Kasen, D., Howell, D. A., Bersier, D., Bloom, J. S., Kulkarni, S. R., Kandrashoff, M. T., Filippenko, A. V., Silverman, J. M., Marcy, G. W., Howard, A. W., Isaacson, H. T., Maguire, K., Suzuki, N., Tarlton, J. E., Pan, Y.-C., Bildsten, L., Fulton, B. J., Parrent, J. T., Sand, D., Podsiadlowski, P., Bianco, F. B., Dilday, B., Graham, M. L., Lyman, J., James, P., Kasliwal, M. M., Law, N. M., Quimby, R. M., Hook, I. M., Walker, E. S., Mazzali, P., Pian, E., Ofek, E. O., Gal-Yam, A., & Poznanski, D. 2011, *Nature*, 480, 344
- Paxton, B., Bildsten, L., Dotter, A., Herwig, F., Lesaffre, P., & Timmes, F. 2011, *ApJS*, 192, 3
- Perets, H. B., Badenes, C., Arcavi, I., Simon, J. D., & Gal-yam, A. 2011, *ApJ*, 730, 89
- Perets, H. B., Gal-Yam, A., Mazzali, P. A., Arnett, D., Kagan, D., Filippenko, A. V., Li, W., Arcavi, I., Cenko, S. B., Fox, D. B., Leonard, D. C., Moon, D.-S., Sand, D. J., Soderberg, A. M., Anderson, J. P., James, P. A., Foley, R. J., Ganeshalingam, M., Ofek, E. O., Bildsten, L., Nelemans, G., Shen, K. J., Weinberg, N. N., Metzger, B. D., Piro, A. L., Quataert, E., Kiewe, M., & Poznanski, D. 2010, *Nature*, 465, 322
- Piro, A. L. 2012, *ArXiv e-prints*
- Poznanski, D., Chornock, R., Nugent, P. E., Bloom, J. S., Filippenko, A. V., Ganeshalingam, M., Leonard, D. C., Li, W., & Thomas, R. C. 2010, *Science*, 327, 58
- Shen, K. J. & Bildsten, L. 2009, *ApJ*, 699, 1365
- Shen, K. J., Kasen, D., Weinberg, N. N., Bildsten, L., & Scannapieco, E. 2010, *ApJ*, 715, 767
- Sim, S. A., Fink, M., Kromer, M., Röpke, F. K., Ruiter, A. J., & Hillebrandt, W. 2012, *MNRAS*, 420, 3003
- Sim, S. A., Röpke, F. K., Hillebrandt, W., Kromer, M., Pakmor, R., Fink, M., Ruiter, A. J., & Seitzzahl, I. R. 2010, *ApJ*, 714, L52
- Sullivan, M., Kasliwal, M. M., Nugent, P. E., Howell, D. A., Thomas, R. C., Ofek, E. O., Arcavi, I., Blake, S., Cooke, J., Gal-Yam, A., Hook, I. M., Mazzali, P., Podsiadlowski, P., Quimby, R., Bildsten, L., Bloom, J. S., Cenko, S. B., Kulkarni, S. R., Law, N., & Poznanski, D. 2011, *ApJ*, 732, 118
- Tanaka, M., Mazzali, P. A., Benetti, S., Nomoto, K., Elias-Rosa, N., Kotak, R., Pignata, G., Stanishev, V., & Hachinger, S. 2008, *ApJ*, 677, 448
- Timmes, F. X., Hoffman, R. D., & Woosley, S. E. 2000a, *ApJS*, 129, 377
- Timmes, F. X. & Niemeyer, J. C. 2000, *ApJ*, 537, 993
- Timmes, F. X., Zingale, M., Olson, K., Fryxell, B., Ricker, P., Calder, A. C., Dursi, L. J., Tufo, H., MacNeice, P., Truran, J. W., & Rosner, R. 2000b, *ApJ*, 543, 938
- Waldman, R., Sauer, D., Livne, E., Perets, H., Glasner, A., Mazzali, P., Truran, J. W., & Gal-Yam, A. 2010, *ArXiv e-prints*
- Woosley, S. E. & Kasen, D. 2011, *ApJ*, 734, 38
- Woosley, S. E. & Weaver, T. A. 1994, *ApJ*, 423, 371
- Zingale, M., Dursi, L. J., Zuhone, J., Calder, A. C., Fryxell, B., Plewa, T., Truran, J. W., Caceres, A., Olson, K., Ricker, P. M., Riley, K., Rosner, R., Siegel, A., Timmes, F. X., & Vladimirova, N. 2002, *ApJS*, 143, 539